ELSEVIER

Tectonophysics 265 (1996) 181–190

TECTONOPHYSICS

Observation and modelling of the Saint-Étienne-de-Tinée landslide using SAR interferometry

B. Fruneau, J. Achache *, C. Delacourt

Département Etudes Spatiales, Institut de Physique du Globe de Paris 4, place Jussieu, 75252 Paris, France

Received 16 October 1995; accepted 11 March 1996

Abstract

Six different interferograms of the "La Clapière" landslide were derived from ERS-1 SAR images during the period Aug. 20–Sept. 4, 1991. The coherence of the associated images is shown to remain significant over most of the surface of the landslide during the two weeks of the survey. The interferograms are remarkably similar, and indicate steady-state displacements over at least 12 days. The displacement field derived from the interferograms is shown to be characterized by a non-uniform displacement gradient from top-to-bottom and reveals a significantly faster motion of the western part of the landslide. The amplitude of the motion deduced from interferometry is shown to be in good agreement with ground measurements. Finally, SAR interferometry is shown to be able to evidence small-scale instabilities which may not be observed with discrete ground measurements.

1. Introduction

SAR interferometry has proved its ability to detect and map surface displacements over tens-of-kilometers-wide areas with centimeter-scale accuracy. This was demonstrated by Massonnet et al. (1993, 1994), in the case of the Landers earthquake, where changes in range from the ground surface to the satellite have been shown to be consistent with the deformation computed using an elastic dislocation model. The same area was studied by Zebker et al. (1994) and also by Peltzer et al. (1994) who examined displacements in the vicinity of the rupture fault which could not be accounted for by the above model. Goldstein et al. (1993) also used SAR interferometry to detect sea ice motion in Antarctica. More recently, Massonnet et al. (1995) produced a series of interferograms on Mount Etna. The corresponding deformation was shown to be compatible with the relaxation of the edifice following the eruption of 1991–1993. All these studies deal with large-scale surface deformation mapping.

Using a couple of SAR images acquired above southern France by ERS-1, we were able to detect a 1-km^2 landslide at Saint-Étienne-de-Tinée (Fruneau and Achache, 1995). This study demonstrated the capability of SAR interferometry to map surface displacements on a very small scale, characteristic of landslides, as well as volcanic slopes. In this preliminary study based on a single interferogram, the displacement field was shown to be consistent with an essentially plastic behaviour of the landslide with elastic deformation localised near the major structural discontinuities. In the present paper, we con-

* Corresponding author. Tel.: +33-1-4427-2405; Fax: +33-1-4427-3373.

PII S0040-1951(96)00047-9

duct a more extensive study of this landslide based on five different interferograms constructed over a period of two weeks using five different ERS-1 images.

2. The landslide

The Mercantour massif, in the French Alps, is the site of a 1 km^2 landslide (44.25°N, 6.96°E) which extends between 1100 and 1700 m in altitude on the left bank of the Tinée river, downstream the village of Saint-Étienne-de-Tinée. A detailed description of the morphology and history of the landslide can be found in Follacci (1987). It is bounded at the top by a 70-m-high scarp displaying two lobes (Fig. 1). A second scarp, more developed on the northwest (left) side of the landslide, is observed at mid-level. The steepest slopes are observed in the lower part of the landslide, below a competent layer of migmatites known as the "barre d'Iglière" near the 1300–1500 m altitude which produces a subhorizontal mechanical discontinuity.

The landslide has been monitored by inclinometry since 1979 and by laser-ranging since 1982. A permanent network of 50 laser targets is currently deployed on the landslide. These measurements have evidenced displacements of the order of 13 m between the end of 1982 and the end of 1986 with a peak value of 2.5 m in one month during the crisis of 1986–1987. Displacements are currently of the order of 1–2 cm/day. The overall parallelism of the directions of motion and the synchronism of the seasonal accelerations support the hypothesis of a deep phenomenon (Follacci, 1987). According to this author, the landslide can be partitioned into three different zones, separated by two sub-vertical faults trending N20°. The behaviour of these zones ranges from polyhedral slip, in the northwest, to rotational slip in the southeast (Follacci et al., 1988).

3. Coherence analysis

SAR images of the landslide were acquired by ERS-1 with a 3-day repeat cycle, during the Com-

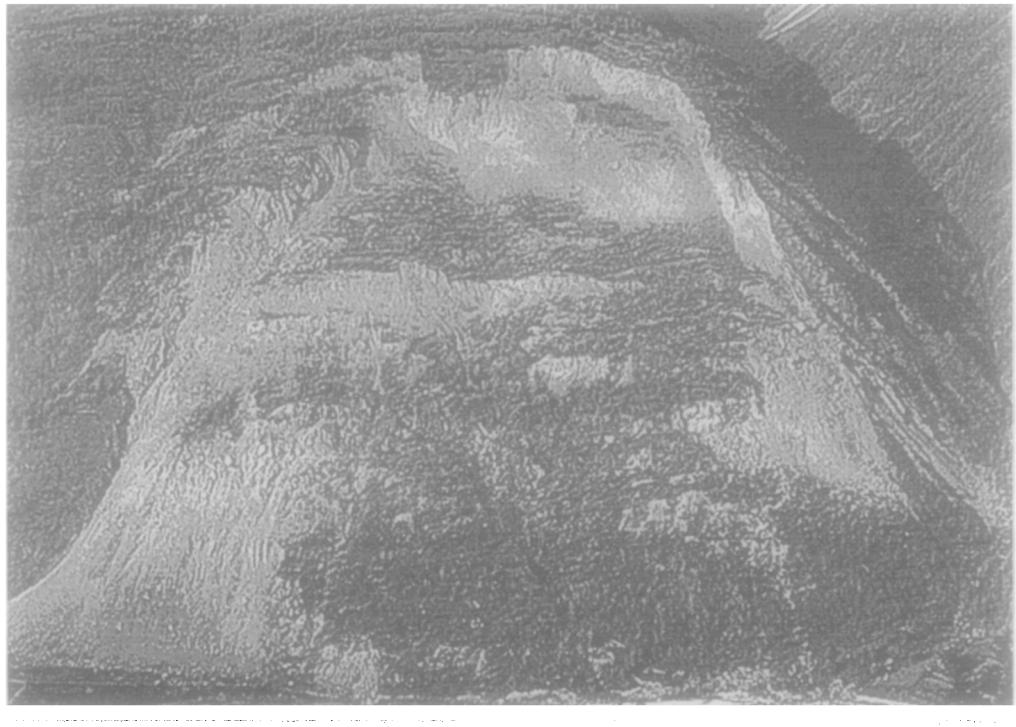

Fig. 1. The "La Clapière" landslide. Slope azimuth is N205°. Major faults are trending N20°.

missioning Phase (CP) on descending orbits and during the two Ice Phases (IP) on ascending orbits. Images were also produced with a 35-day repeat cycle, during the Multidisciplinary Phase (MP). Given the amplitude of the ground displacements anticipated (of the order of 1 cm/day) and the presence of vegetation on the slope, the present study focuses on images obtained with a high repeatability, i.e. taken during CP or IP. Furthermore, images acquired during CP on descending orbits provide the appropriate exposure for studying westward looking slopes and are therefore best suited for studying the "La Clapière" landslide. On the contrary, given the gradient value (40°) and the slope azimuth (N 205°), images from the landslide acquired on ascending passes will be plagued by layover. Five images acquired during CP on August 20, 23, 26, 29 and September 4, 1991, were selected.

Table 1
Estimated normal baseline (in meters) for the 10 possible pairs

	Aug. 23	Aug. 26	Aug. 29	Sept. 04
Aug. 20	−591	−545	−4	−301
Aug. 23		43	587	291
Aug. 26			543	248
Aug. 29				−298

Among the ten pairs of images that can be used to generate interferograms with these five images, only six have baseline values sufficiently low (Table 1). Indeed, with the radar characteristics of ERS-1, base-

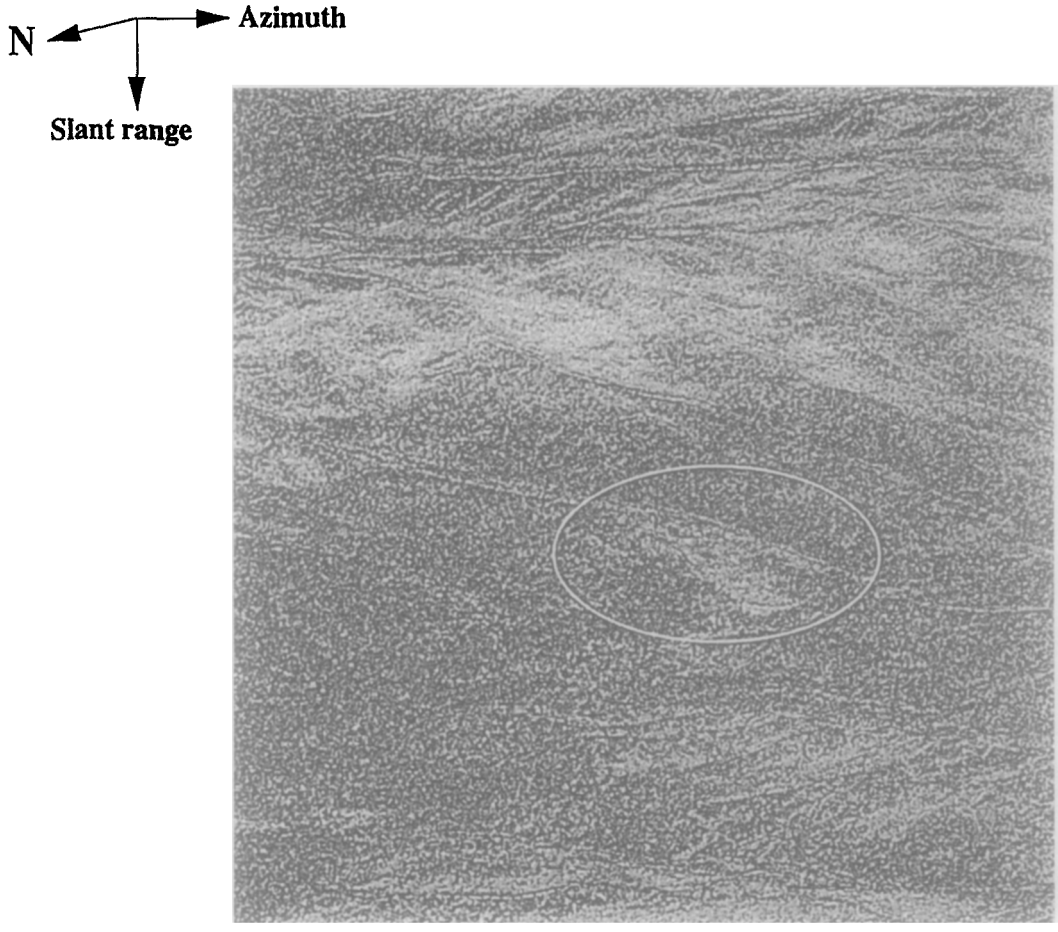

Fig. 2. Coherence of pair 23–26. Its dimension is 1024 × 1024 pixels. Each pixel size is about 9 m (slant range) × 4 m (azimuth). The ellipse indicates the area of the landslide. The normal baseline is 43 m.

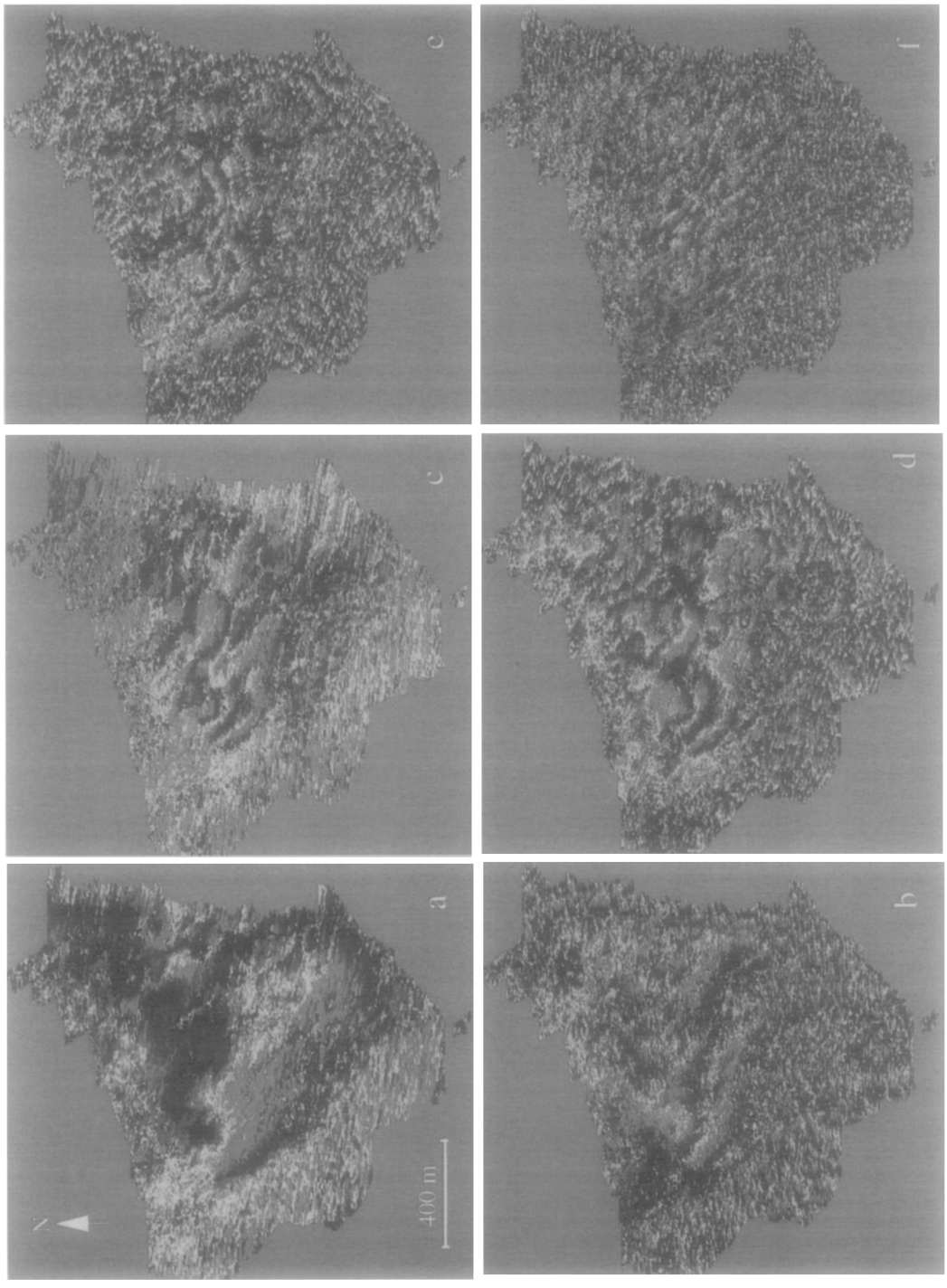

Fig. 3. (a) Geocoded interferogram 23–26. Normal baseline: 43 m. (b) Geocoded interferogram 29–04. Normal baseline: −298 m. (c) Geocoded interferogram 20–29. Normal baseline: −4 m. (d) Geocoded interferogram 26–04. Normal baseline: 248 m. (e) Geocoded interferogram 23–04. Normal baseline: 291 m. (f) Geocoded interferogram 20–04. Normal baseline: −301 m.

lines in excess of 500 m are not appropriate for interferometry (Zebker and Villasenor, 1992).

The coherence between these images appears to be higher at higher altitude (Fig. 2) suggesting that coherence loss is primarily associated with vegetation (alpine forest) which is more developed at low altitude. Coherence is also high on the landslide where the rock surface is more exposed: the NW part of the slide, corresponding to the active scree slope, appears as the most coherent part of the slide. This may also indicate that no major rockfalls occurred during the period of survey.

The coherence is still significant for the Aug. 20–Sept. 4 pair, indicating that landslide interferograms can still be obtained with a 15-day repeat cycle. Coherence for 35-day pairs appears to be much lower, thus preventing any interferogram to be generated from images acquired during the multidisciplinary phase. This allows us to set an a priori limit to interferogram production somewhere between 15 and 30 days in areas covered by vegetation.

4. Interferogram production

Interferograms are generated on a TMC (Thinking Machine Corporation) massively parallel computer CM5-128. The coregistration of the images is performed by maximising the correlation between the two images at a large number of tie-points (typically 1000 for a 20 km × 20 km image) evenly distributed throughout the scene. The geometric deformation is obtained by matching second-order polynomials to the values obtained at each tie-point (Delacourt et al., 1995).

The effect of topography is removed using a 5 m × 5 m Digital Elevation Model (DEM) provided by the Institut Géographique National (IGN) of France, in Lambert 3 coordinates. This is the easiest approach for constructing differential interferograms, and then the deformation field, when a DEM is available. The interferograms are projected on the DEM. Finally, a self-adaptative filter specifically developed for SAR interferograms (Delacourt et al., 1995) is applied to improve the signal-to-noise ratio. Fig. 3 displays the six geocoded filtered interferograms obtained.

5. Interferogram analysis

Significant phase variations (fringes) associated with the landslide can be easily detected on at least five of these interferograms. The 23-26 interferogram (Fig. 3a), which corresponds to the highest coherence, associated with a baseline of 40 m and a very short time interval (3 days), provides the clearest picture of the landslide. The limits of the slide are clearly evidenced, especially the northwestern boundary and the 2 lobes at the top. It very distinctly reveals deformation fringes associated with the landslide. The 29-04 pair (Fig. 3b) leads to a more noisy interferogram, as could have been expected from its lower coherence and large baseline (298 m). Fig. 3c and d display the 20-29 and 26-04 interferograms, both corresponding to a 9 days interval. Both interferograms display clear and consistent fringe systems, in particular in the northwestern half of the landslide where coherence is highest. The SNR of the 23-04 interferogram (Fig. 3e) is lower than for the other interferograms, presumably due to the larger elapsed time (12 days) and the value of the baseline (291 m). It is, however, sufficient to reveal the presence of fringes, their overall NW–SE trend as well as their curvature on the western side of the slide. In the 20-04 interferogram (Fig. 3f), the existence of phase variations within the landslide can still be detected but the fringes geometry cannot be recovered. Wether this reduction in SNR is due to the elapsed time (15 days) or to the baseline (301 m) is unclear and this study does not rule out the possibility that the St-Étienne-de-Tinée landslide can be monitored by interferometry over more than two weeks.

The interferogram 20-29 is characterised by a very short baseline (see Table 1), i.e. a very large altitude of ambiguity: this represents an almost ideal case where the two passes of the satellite shared the same orbit. Even prior to the flat terrain correction, the interferogram displays two clearly distinct fringe systems. The effect of topography, corresponding to the largest fringes cannot be confused with the signature of surface displacements localised on the landslide. Indeed, in this case, a 2π phase rotation corresponds either to a few cm of displacement or more than 1000 m of topography (see Fruneau and Achache, 1995).

One observes in Fig. 3 the similitude of the different interferograms. The number of fringes increases almost linearly with the time interval covered by the interferograms, while their overall geometry remains similar. In particular, interferograms 20-29 and 26-04 (Fig. 3c and d), built with images taken 9 days apart, but from two independent pairs of images, are strikingly similar. This is particularly clear, again, in the western part, where the fringes can be most clearly evidenced. This suggests that the observed landslide motion is stationary over the period surveyed.

On all the interferograms, NW–SE-trending fringes attest of a downhill movement characterised by a gradient of displacement from the top to the bottom of the landslide. The sense of the phase rotation indicates that the motion decreases towards the bottom. A full phase rotation (one fringe) is equivalent to a displacement gradient of 2.8 cm along the line-of-sight of the radar, or 3.9 cm along the landslide average steepest slope.

In the western part of the landslide, which corresponds to the active scree slope, interferograms display a clear pattern of curved, almost parallel, fringes. Elsewhere, the fringe intervals are not constant over the landslide, suggesting both vertical and lateral variations of the displacement gradient. From the active scree slope towards the southeast, i.e. towards the right side of the landslide, one observes a progressive increase of the fringe separation, indicating a progressive decrease of the displacement gradient. This pattern is common to all interferograms. The gradient of displacement changes also from top-to-bottom, especially in the southeastern part: the gradient is very low between the intermediate scarp and the "barre d'Iglière" and seems to increase below this layer. This is consistent with the hypothesis that the "barre d'Iglière" behaves as a competent mechanical layer that blocks the movement and maintains some coherence in the upper part of the massif.

6. Modelling

Since interferograms measure only one component of the displacement (its projection on the slant-range), recovering the three components of the displacement field requires some a priori hypotheses on the mechanical behaviour of the landslide. Synthetic interferograms have been computed for two different sliding models which represent the most important types of slope failure: rotational and translational slips (Bromhead, 1986; Giani, 1992). In rotational slip, the sliding surface has a spoon shape, and can be approximated by a circle in vertical cross-section. With translational slip, the failure surface tends to be planar and roughly parallel to the slope.

6.1. Rotational model

The surface displacements associated with this model are similar to the simple tilt of a rigid block. As already shown by Peltzer et al. (1994), we observe that the fringe separation is not sensitive to the curvature of the sliding surface and only depends on the rotation of the block. With such a model, the interferogram analysis appears therefore not to be efficient to estimate the depth of the sliding surface, a parameter which controls the behaviour of the landslide and the related hazard. In any case, this type of model does not seem to describe the St-Étienne-de-Tinée landslide since it shows fringes with a regular spacing interval and cannot account for the observed non-uniform gradients displayed by the interferograms.

Fig. 4. (a) Synthetic interferogram based on model 2. A top-to-bottom gradient of displacement is gradually decreased across the landslide from 1.5 cm/100 m in the northwest to 0.5 cm/100 m in the southeast. This interferogram should be compared with the 3 days interferogram of Fig. 3a. (b) The displacement field is increased be a factor 2 with respect to (a). To be compared with the 6 days interferogram of Fig. 3b. (c) The displacement field is increased by a factor 3 with respect to (a). To be compared to the 9 days interferograms of Fig. 3c and d. (d) The displacement field is increased by a factor 4 with respect to (a). To be compared to the 12 days interferogram of Fig. 3e.

Fig. 5. Difference between the real and the modeled interferogram.

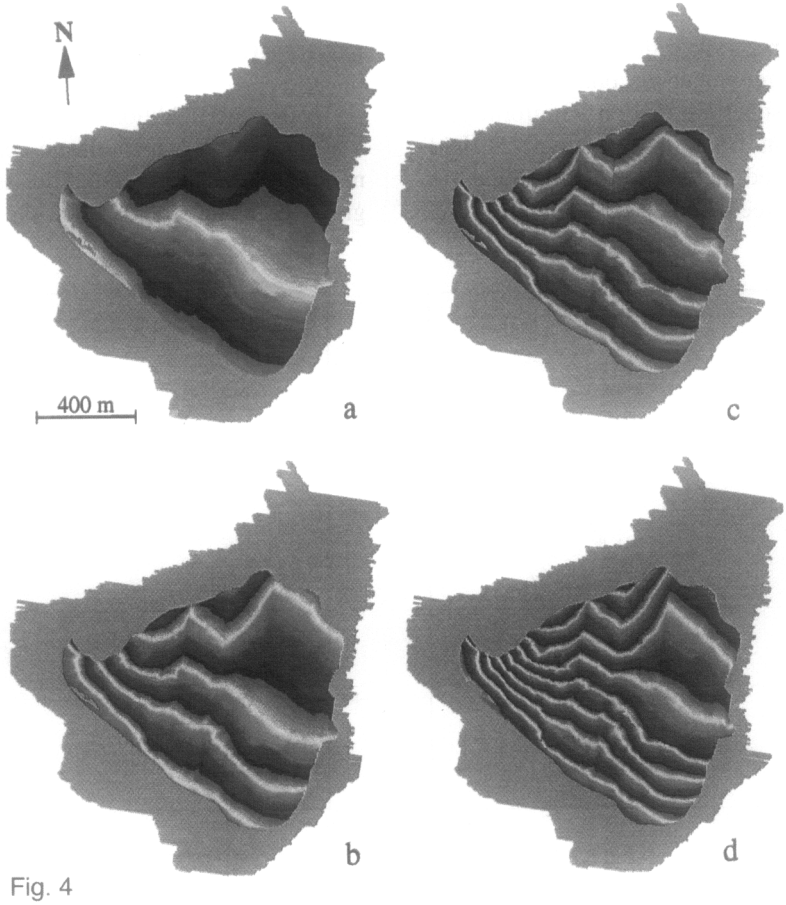

Fig. 4

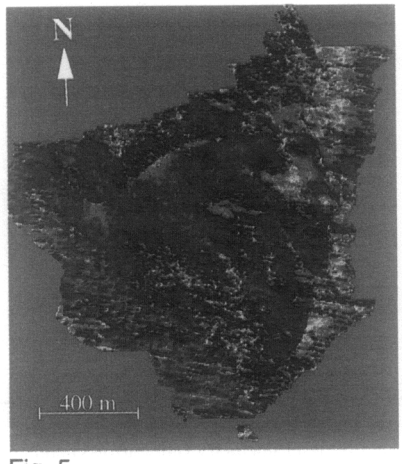

Fig. 5

6.2. Planar model

A preliminary model based on the 20-29 interferogram (Fig. 3c) was proposed in a previous study (Fruneau and Achache, 1995). In this model, elastic deformation along three major discontinuities (faults trending N20°) was superimposed on a uniform gradient of displacement from top-to-bottom. A rigid block of a few hundred meters was also included in the eastern part, between the "barre d'Iglière" and the intermediate scarp. However, when the amplitude of the displacements is rescaled assuming a constant velocity field, this model cannot account for the fringes observed on the new 3, 6 and 12 days interferograms derived in the present paper (Fig. 3a, b, e).

Using these additional interferograms, we derived a new model in which elastic deformation along the major structural discontinuities is modelled by progressive lateral decrease of the top-to-bottom dis-

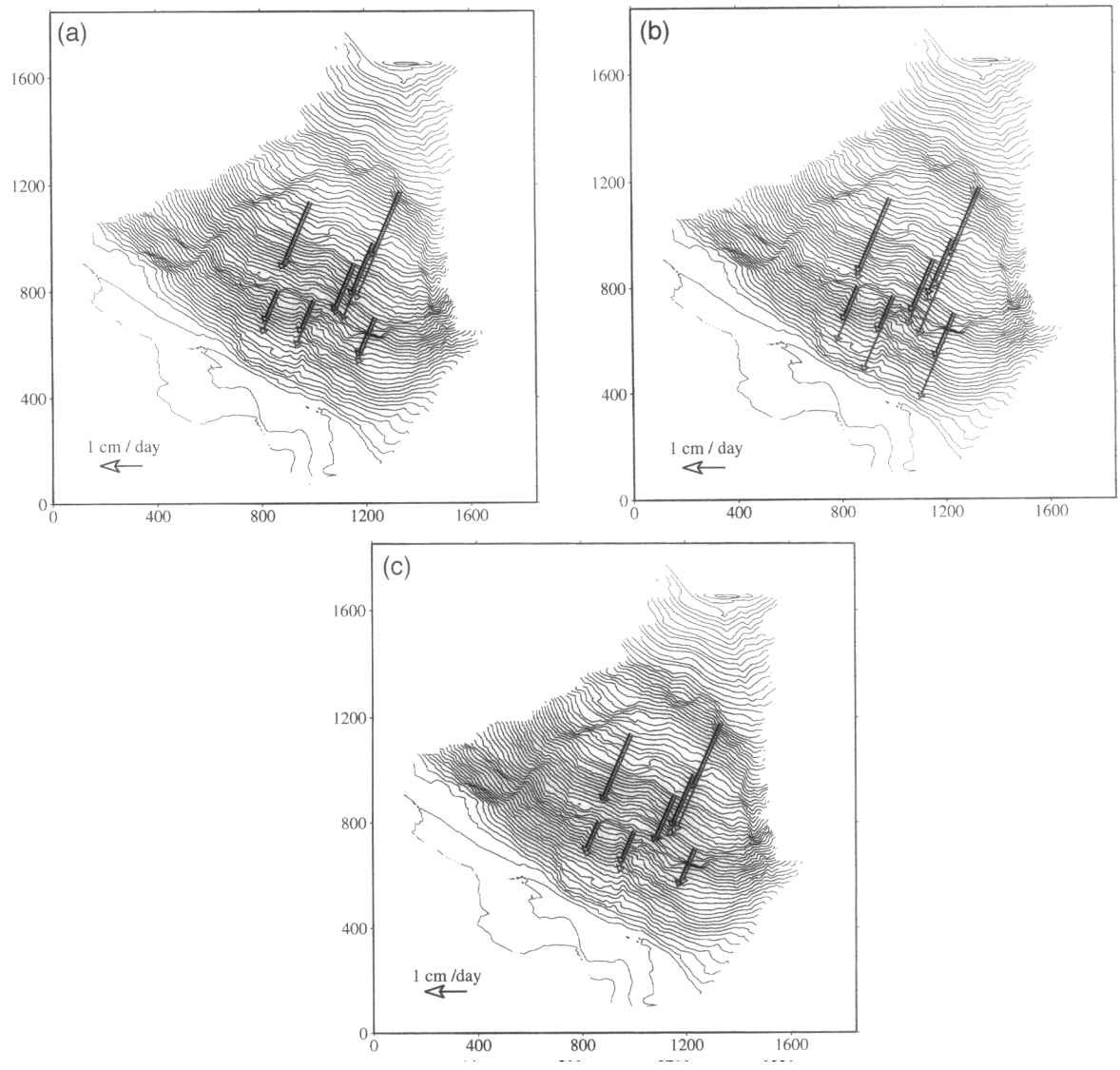

Fig. 6. (a) Displacement vector measured on ground by laser telemetry (grey arrows) and computed from the model (black arrows) for the 26–04 period. (b) Same as (a) for the 23–26 period. (c) Same as (a) for the 20–29 period.

placement gradient. Fig. 4a displays synthetic fringes produced by such a displacement field with a gradient ranging from 1.5 cm/100 m in the western part of the slide to 0.5 cm/100 m in the east above the barre d'Iglière and 1 cm/100 m below the barre. This variation of the gradient of displacement from the top to the bottom was introduced to further improve the fit between observed and synthetic fringes in the eastern part of the landslide. It may be associated with a swelling of the topography above the "barre d'Iglière" and is consistent with the mechanical behaviour of this layer which holds back the upper part of the landslide. This interferogram (Fig. 4a) can be compared with the 23-26 interferogram (Fig. 3a). The displacement field of Fig. 4a can, then, be rescaled by factors 2, 3 and 4 and the resulting fringes (Fig. 4b, c and d) can be readily compared with the 6, 9 and 12 days interferograms of Fig. 3b, c and e, showing a satisfactory agreement.

Fig. 5 displays the difference between modelled and observed fringes of the 23-26 pair. We observe a nearly uniform phase value over the area of the landslide, indicating a good agreement between the two interferograms over most of the sliding zone. At the eastern top of the slide, Fig. 5 displays significant phase variations over a small area. This evidences a small unit in the landslide which displacement is not taken into account by the above model. One of the laser targets located in this area indeed confirms the existence of a rapid movement. Fig. 5 also reveals the increasing noise of the real interferogram towards the bottom of the slide.

7. Comparison with ground measurements

During the period of the study, daily ground measurements have been performed on five laser targets of the network operated on the landslide. As discussed above, the interferometric analysis of the landslide evidences a steady-state displacement field over at least 12 days. It also indicates that this displacement field is dominated by a top-to-bottom gradient. The measurements collected on the ground for the different periods of the surveys confirm the existence of this gradient. As discussed above, they also confirm an anomalously high displacement of the upper east part (Fig. 6). Some discrepancies are observed on a few targets, in particular for the 23-26 period (Fig. 6b). These discrepancies may be attributed to the great sensitivity of laser measurements, which are available at a discrete number of points, to local heterogeneities, on short time-scales. In comparison, interferometry provides a more continuous description of the deformation field both in time and space. It allows, in particular, to delineate the limits between the different units of the landslide.

Interferograms provide only the gradients of the displacements and the displacement of the bottom of the landslide with respect to the surrounding bedrock was arbitrary set to zero in our model. Ground displacements recorded at a few critical points are therefore necessary to complement SAR analysis and determine absolute displacements. In the present case, ground measurements by laser telemetry reveal a systematic offset with the average displacement recorded by SAR interferometry. This offset varies from 2 to 7 mm/day over the duration of the survey and provides an estimate of the absolute displacement at the bottom of the landslide.

8. Conclusions

SAR interferometry demonstrated its capability for studying the deformation over small areas. We were able to construct several interferograms on which the landslide is clearly evidenced. These interferograms show an organised fringe system for an elapsed time as large as 12 days, allowing us to construct a steady-state model of surface displacements valid for the whole period of observation. A simple model of translational slide satisfactorily accounts for the observed interferogram, and suggests the existence of a significant plastic deformation in the vicinity of the N20° structural discontinuities cutting the slide. The influence of the major heterogeneities of the landslide ("barre d'Iglière", intermediate scarp) on its mechanical behaviour can also be constrained by the interferometric analysis. It also provides accurate estimates of the displacement gradients in agreement with ground measurements and even allows us to detect small blocks with enhanced displacement which may represent a potential hazard.

The evidence for a steady-state displacement field presented in this study does not rule out the existence of different modes and velocities of deformation taking place on the landslide at different period as suggested by daily ground measurements. Further observations of the landslide would be necessary to analyse the long-term stability of the proposed deformation model. The ERS tandem experiment which will perform repeated observations with a one-day repeat cycle, provides an unique opportunity for this study. The amplitude of ground displacements is sufficient to be determined during a period of one day. Furthermore, this short time between acquisitions precludes any loss of coherence, thus improving the SNR of interferograms and the accuracy of the determination of the displacement field.

Acknowledgements

We would like to thank the European Space Agency for the ERS-1 SAR images and J.-P. Follaci (CETE, Nice) who provided the displacement values of the landslide measured on the ground. This is IPGP contribution 1435.

References

Bromhead, E.N., 1986. The Stability of Slopes. Blackie, London, 411 pp.

Delacourt, C., Duviols, J.L., Fruneau, B. and Achache, J., 1995. SAR interferometry processing using massively parallel computers. submitted to Computers and Geosciences.

Follacci, J.-P., 1987. Les mouvements du versant de la Clapière à Saint-Étienne-de-Tinée (Alpes-Maritimes). Bull. Liaison Lab. P. Ch., 150/151: 39–54.

Follacci, J.-P., Guardia, P., Ivaldi, J.-P., 1988. Geodynamic framework of the la Clapière landslide (Maritime Alps, France). In: Proc. 5th Int. Symp. Landslides, Lausanne, 10–15 July 1988, pp. 1323–1327.

Fruneau, B. and Achache, J., 1995. Détection du glissement de terrain de Saint-Étienne-de-Tinée par interférométrie SAR et modélisation. C.R. Acad. Sci. Paris, 320, Série IIa: 809–816.

Giani, G.P., 1992. Rock Slope Analysis. Balkema, Rotterdam, 361 pp.

Goldstein, R.M., Engelhardt, H., Kamb, B. and Frolich, R.M., 1993. Satellite radar interferometry for monitoring ice sheet motion: Application to an Antarctic ice stream. Science, 262: 1525–1534.

Massonnet, D., Rossi, M., Carmona, C., Adragna, F., Peltzer, G., Feigl, K. and Rabaute, T., 1993. The displacement field of the Landers earthquake mapped by radar interferometry. Nature, 364: 138–142.

Massonnet, D., Feigl, K., Rossi, M. and Adragna, F., 1994. Radar interferometric mapping of deformation in the year after the Landers earthquake. Nature, 369: 227–230.

Massonnet, D., Briole, P. and Arnaud, A., 1995. Deflation of Mount Etna monitored by spaceborne radar interferometry. Nature, 375: 567–570.

Peltzer, G., Hudnut, K.W. and Feigl, K.L., 1994. Analysis of coseismic surface displacement gradients using radar interferometry: New insights into the Landers earthquake. J. Geophys. Res., 99: 21,971–21,981.

Zebker, H.A. and Villasenor, J., 1992. Decorrelation in interferometric radar echoes. IEEE Trans. Geosci. Remote Sensing, 30: 950–959.

Zebker, H.A., Rosen, P., Goldstein, R.M., Gabriel, A. and Werner, C.L., 1994. On the derivation of coseismic displacement fields using differential radar interferometry: the Landers earthquake. J. Geophys. Res., 99: 19,617–19,634.